Iridium(III) Complexes with Fluorinated Phenyl-tetrazoles as Cyclometalating Ligands: Enhanced Excited-State Energy and Blue Emission [‡]

Andrea Baschieri*,[a] Letizia Sambri,[b] Andrea Mazzanti,[b] Armando Carlone,[a] Filippo Monti*,[c] and Nicola Armaroli[c]

[a] Dipartimento di Scienze Fisiche e Chimiche, Università degli Studi dell'Aquila, Via Vetoio, 67100 L'Aquila, Italy

[b] Dipartimento di Chimica Industriale "Toso Montanari", Università di Bologna, Viale Risorgimento 4, 40136 Bologna, Italy

[c] Istituto per la Sintesi Organica e la Fotoreattività, Consiglio Nazionale delle Ricerche, Via P. Gobetti 101, 40129 Bologna, Italy

[‡] Dedicated to the memory of Prof. Giuseppe Bartoli

Supporting Information Placeholder

ABSTRACT: Five cationic iridium(III) complexes with fluorinated cyclometalating tetrazole ligands $[Ir(dfptrz)_2L]^+$, where Hdfptrz = 5-(2,4-difluorophenyl)-2-methyl-2H-tetrazole and L = 2,2'-bypiridine (**1F**), 4,4'-di-tert-butyl-2,2'-bipyridine (**2F**), 1,10-phenanthroline (**3F**), 4,4'-bis(dimethylamino)-2,2'-bipyridine (**4F**), and tert-butyl isocyanide (**5F**) were prepared following a one-pot synthetic strategy based on a bis-cyclometalated solvato-complex obtained via silver(I)-assisted cyclometalation, which was then reacted with the proper ancillary ligand to get the targeted complexes. The X-ray crystal structures of **2F** and **4F** were determined, showing that the tetrazole ligands are in a *trans* arrangement with respect to the iridium center. Electrochemical and photophysical properties, along with density functional theory calculations, allowed a full rationalization of the electronic properties of **1F−5F**. In acetonitrile solution at 298 K, complexes **1F−3F**, equipped with bipyridine and phenanthroline ligands, exhibit strong vibronically structured luminescence bands in the blue region with photoluminescence quantum yields (PLQYs) in the range 56–76%. This behavior is radically different from the non-fluorinated analogues reported previously, which emit in the green region from ^{3}MLCT excited states. **4F** shows relatively strong emission (PLQY = 40%) of charge transfer character centered on the amino-bipyridine ancillary ligand, whereas the emission of **5F** is very weak (PLQY = 0.6%), further blue-shifted and attributed to the lowest ligand-centered (^{3}LC) triplet state of the tetrazolyl cyclometalated moiety. A similar photophysical behavior is observed in PMMA at 298 K, while in 77-K matrix all of the compounds are strong emitters. This novel fluorinated phenyl-tetrazole cyclometalating ligand provides the corresponding iridium(III) complexes with a combination of excited-state energy and redox potentials that make them very promising as photoredox catalysts.

INTRODUCTION

Among the many families of coordination compounds based on transition metals, cyclometalated iridium(III) complexes play a very important role in different applications[1] thanks to their remarkable chemical and thermal stability as well as unique luminescence properties. These compounds may exhibit emission colors across the entire chromatic scale,[2-4] with typically very high emission quantum yields.[5, 6] Accordingly, cyclometalated iridium(III) complexes are commonly used as pH sensors,[7] probes for biological and optical imaging, [8] tools for medical diagnostics,[9, 10] photocatalysts[11-13] and photosensitizers in outer-sphere electron transfer reactions.[14] Probably, their most popular application is serving as emissive dopants in multicolor electroluminescent displays based on organic light emitting diodes (OLEDs)[15] and light-emitting electrochemical cells (LECs).[16-18] In fact, many examples of highly efficient iridium-based phosphors displaying green and red emission are known and even used in commercial applications.[15] On the contrary, suitable blue-emitting analogues are not readily available, mainly because such complexes do not possess sufficiently high photoluminescence quantum yields or exhibit unsatisfactory Commission International de l'Éclairage (CIE) color coordinates.[19, 20]

In order to obtain blue iridium(III) emitters, several strategies can be implemented.[1, 15, 16] One of the most effective approaches is the stabilization of the HOMO, which can be obtained by different strategies: (i) addition of electron-withdrawing groups, typically fluorine, to the aryl moiety of the cyclometalated ligand;[21] (ii) reduction of the ring size of the aromatic N-heterocycle and increase of the number of nitrogen atoms.[22, 23] The latter approach has been well investigated and several examples of iridium(III) complexes with cyclometalating ligands entailing 5-membered nitrogen heterocycles have been reported (*e.g.*, 1-aryl-1,2-pyrazoles,[24] phenyl imidazoles,[25] and even few types of aryl triazoles, like 5-aryl-1,2,4- triazoles[26] and aryl-1,2,3-triazoles).[27]

In this context, we designed and synthesized the first series of iridium(III) complexes bearing a phenyl-tetrazole derivative

as cyclometalating ligand (*i.e.*, Hptz = 2-methyl-5-phenyl-2*H*-tetrazole).[28] Such complexes are reported in Chart 1 for the sake of comparison (*i.e.*, **1H–3H** and **5H**). The emission of this family of

Chart 1. Tetrazole-Based Cyclometalated Iridium(III) Complexes Investigated in the Present Work (1F–5F) and in our Previous Publication (1H–3H and 5H).[28]

X = F   [Ir(dfptrz)₂(bpy)]⁺   **(1F)**
X = H   [Ir(ptrz)₂(bpy)]⁺   **(1H)**

X = F   [Ir(dfptrz)₂(dtbbpy)]⁺   **(2F)**
X = H   [Ir(ptrz)₂(dtbbpy)]⁺   **(2H)**

X = F   [Ir(dfptrz)₂(phen)]⁺   **(3F)**
X = H   [Ir(ptrz)₂(phen)]⁺   **(3H)**

[Ir(dfptrz)₂(dmabpy)]⁺   **(4F)**

X = F   [Ir(dfptrz)₂(CN*t*Bu)₂]⁺   **(5F)**
X = H   [Ir(ptrz)₂(CN*t*Bu)₂]⁺   **(5H)**
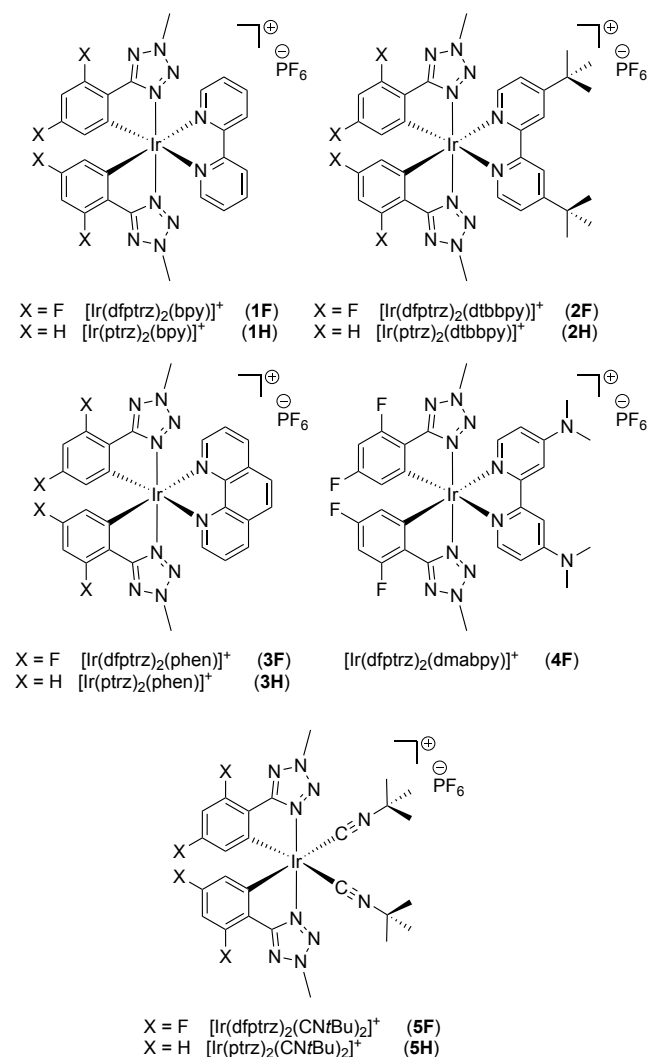
compounds is shifted to the blue region, if compared to cationic iridium(III) complexes equipped with the same ancillary ligands in combination with the more common 2-phenylpyridine (*i.e.*, Hppy) or 2-(2,4-difluorophenyl)pyridine (*i.e.*, Hdfppy) as cyclometalating units.[28] Notably, **1H–3H** were known to

display the highest-energy ³MLCT emission ever reported for fluorine-free cationic cyclometalated iridium(III) complexes.[28] Avoiding the use of fluorine substituents is a key feature to obtain stable blue-emitting electroluminescent devices, because the presence of $C(sp^2)-F$ bonds normally leads to complex degradation under the device operating conditions.[29-31] Anyhow, it must be emphasized that fluorinated complexes are typically stable and perfectly suited for other applications not entailing the use of strong electric fields on the iridium-based emitter.

Taking advantage of the high-energy excited states of these tetrazole-based iridium(III) complexes and of their favorable redox properties, we successfully explored them also as visible-light photoredox catalysts for the formation of new C–C bonds under extremely mild reaction conditions.[32]

In order to further explore the potential of tetrazole-based iridium(III) complexes in the realm of photoredox catalysis, we wanted to push the photo-electrochemical properties of this class of coordination compounds to the limit, by further increasing the HOMO–LUMO gap and the energy of their lowest excited states. To achieve this goal, we took advantage of the fluorine substituents on the phenyl moiety of the cyclometalating ligand. Accordingly, we prepared the 5-(2,4-difluorophenyl)-2-methyl-2*H*-tetrazole ligand (*i.e.*, Hdfptrz) and designed a new series of cyclometalated tetrazole-based iridium(III) complexes (*i.e.*, **1F–5F** in Chart 1). The results of this investigation are presented and discussed herein.

■ **RESULTS AND DISCUSSION**

Synthesis. Based on our previous work,[28, 33-35] we designed a new *N*-substituted 5-phenyltetrazole as cyclometalating ligand (5-(2,4-difluorophenyl)-2-methyl-2*H*-tetrazole, **III,** Scheme 1), equipped with two electron withdrawing fluorine atoms on the aryl moiety.

The synthetic route to obtain **III** is reported in Scheme 1. Tetrazole intermediate **II** was prepared in good yields (80%) from commercially available 2,4-difluorobenzonitrile (**I**) with sodium azide in the presence of ZnCl₂ and acetic acid as catalysts. After 6 hours the white product was recovered by simple filtration in essentially pure form. The treatment of **II** with methyl iodide in the presence of NaOH led to the formation of two methylated derivatives. The desired product can be successfully separated from the undesired isomer 5-(2,4-difluorophenyl)-1-methyl-1*H*-tetrazole by flash chromatography. Through one-dimensional (1D) NOE NMR experiments, centered on the methyl signal, the exact structure of both isomers was confirmed. Compound **III** could be isolated in 45% yield.

Scheme 1. Synthesis of the cyclometallating ligand (III) and of the related complexes (1F–5F).
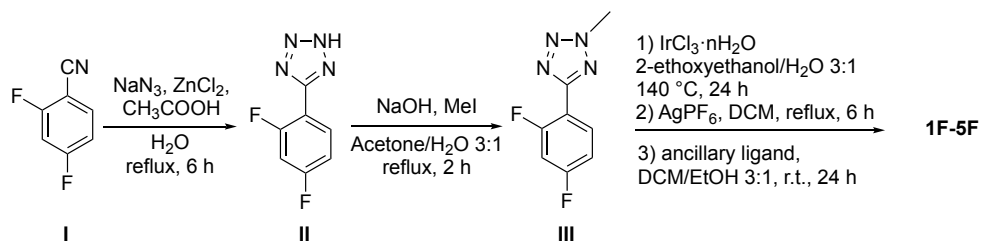
As already described for fluorine-free phenyl-tetrazole derivatives, any attempt to obtain the classical cyclometalated iridium(III) μ-dichloro bridged dimer failed, due to the formation of an $IrCl_3$-tetrazole salt.[28] Therefore, to promote cyclometalation a step involving silver(I) is required. Silver(I) promotes the halide extraction and removes chlorine atoms from the reaction medium, making the iridium core more reactive. The effectiveness of this method, along with the simplicity of the procedures, allowed the reaction to be carried out one-pot.

The tetrazole ligand **III** was reacted with $IrCl_3 \cdot nH_2O$ in a refluxing mixture of 2-ethoxyethanol/water in 3:1 v/v ratio. The obtained yellow salt was filtered off and refluxed in DCM in the presence of $AgPF_6$ in order to obtain the related solvato-complex. The solvato-complex was then reacted with the proper ancillary ligand, in order to prepare the desired complexes **1F–5F**, as reported in Scheme 1. After purification of the crudes by column chromatography on neutral alumina, **1F–5F** were obtained in 46-54% yields.

X-ray Characterization. Slow diffusion of Et_2O vapour in a solution of **2F** and **4F** in CH_3CN gave crystals suitable for X-ray diffraction analysis. The structures of the complexes are reported in Figure 1 and the related crystallographic data are summarized in Table S1.
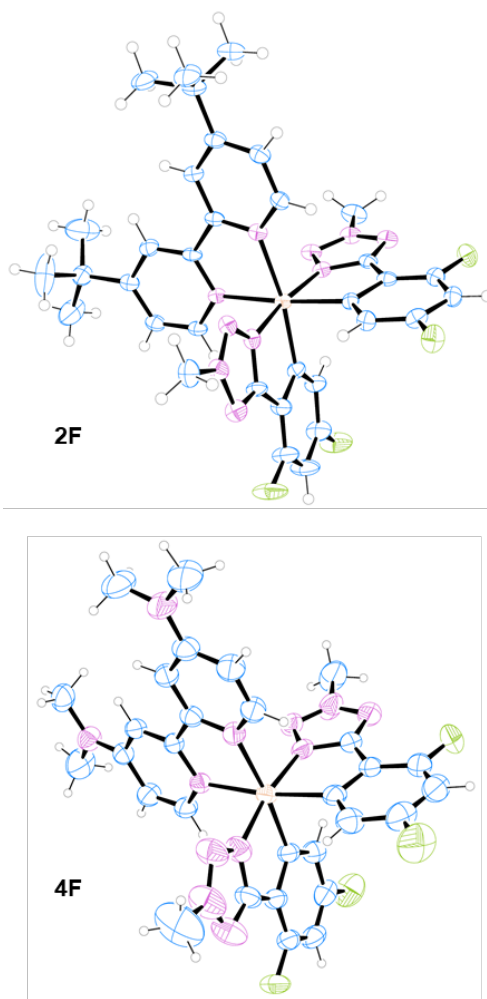
Figure 1. Experimental X-ray structure of complex **2F** and **4F**. ORTEP representations are at the 50% and 30% probability for **2F** and **4F**, respectively. Counter anions and solvents are omitted for clarity.

Complex **2F** crystallizes in the monoclinic $P2_1/c$ space group, while **4F** (as trifluoroacetate salt) belongs to the $P2_1/c$ space group. As already reported in the crystal structure of **2H**,[28] in both **2F** and **4F** structure, the two nitrogen atoms of the tetrazole ligands are in a *trans* arrangement with respect to the octahedral iridium ion. The ancillary ligand fills the two remaining positions in the plane perpendicular to the *trans* nitrogen atoms. Table 1 summarizes the bond lengths around the iridium metal center. The Ir−N and Ir−C distances are very

3

similar to that of **2H** and other iridium complexes reported in the literature.[36-38]

Table 1. Selected bond lengths (in Å).

	2H	**2F**	**4F**
Ir-N$_{1\text{-tetraz}}$	2.00	2.01	2.01
Ir-C$_1$	2.04	2.04	2.04
Ir-N$_{2\text{-tetraz}}$	2.03	2.03	2.00
Ir-C$_2$	2.03	2.03	2.04
Ir-N$_{1\text{-anc.}}$	2.13	2.12	2.12
Ir-N$_{2\text{-anc.}}$	2.13	2.10	2.11

Therefore, the presence of the fluorine substituents on the tetrazole ligand and the different ancillary ligands do not significantly perturb the complex structure around the iridium ion.[28]

Theoretical Calculation: Ground-State Properties. The molecular geometries and the electronic properties of all the synthesized complexes have been investigated by means of density functional theory (DFT) calculations. The M06 hybrid meta-GGA exchange-correlation functional[39, 40] was used in combination with the 6-31G(d,p) basis set[41] for all the non-metal atoms. On the contrary, the Stuttgart/Cologne relativistic pseudopotential and its related correlation-consistent triple-ζ basis set were adopted for the iridium center.[42] The ground state

geometries of all complexes were fully optimized without symmetry constrains in acetonitrile, using the polarizable continuum model (PCM).[43-45] The quality of the theoretically optimized geometries was evaluated by comparison with the available X-ray crystal structure of complex **2F** and **4F**. In Figure S8 the structural overlap between the X-ray crystal structure of **4F** and the theoretically computed one is reported. No substantial differences are found between the two geometries, as corroborated by the value of the minimized root-mean-square deviation of all the atomic positions except hydrogen atoms (*i.e.*, RMSD = 0.226 Å), proving the effectiveness of the selected computational model.

In Figure 2 are reported the energy diagrams and the frontier molecular orbitals of the investigated series (see Chart 1). For all the complexes, the HOMO is mainly located on the iridium center and on both the phenyl moieties of each cyclometalated ligands, as also observed in the case of the previously published fluorine-free series with phenyl-tetrazoles as cyclometalating ligands.[28] Anyway, it should be noted that the HOMO energy of the present complexes is stabilized by approx. 0.34 eV with respect to the analogues of the fluorine-free series (Figure S9); this is an already well-known effect in cationic iridium(III) complexes when fluorine substituents are attached the phenyl moieties of the cyclometalated ligands.[16, 18]
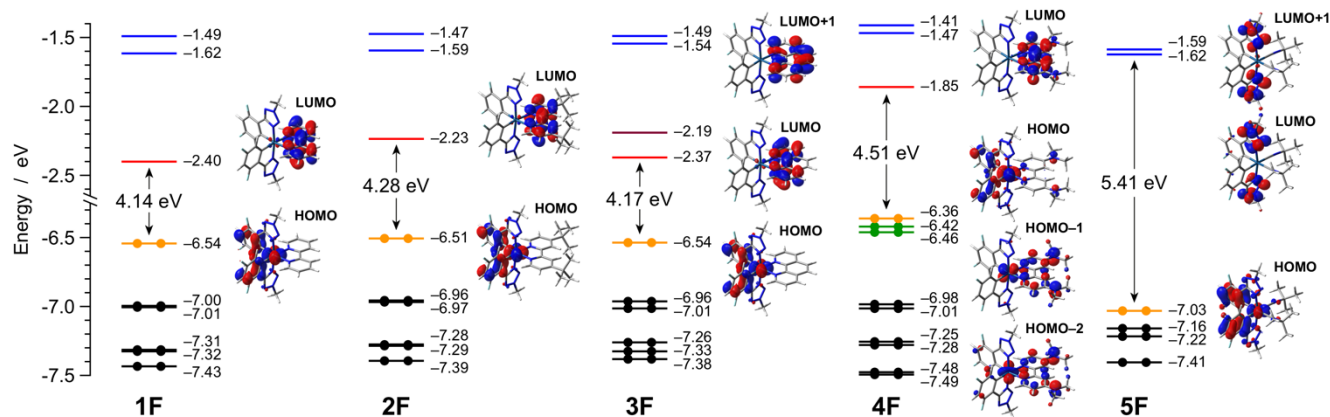

Figure 2. Energy diagram showing the energy values of the frontier Kohn−Sham molecular orbitals of **1F−5F** in acetonitrile. For some relevant orbitals, the corresponding isosurface is also displayed for the sake of clarity (isovalue = 0.04 e$^{1/2}$ bohr$^{−3/2}$). Along the series, relevant orbitals with similar topology are plotted with the same color for an easier comparison.

Within the fluorinated Ir-dfptrz series, in complex **4F**, the strongly electron-donating dmabpy ancillary ligand leads to a HOMO destabilization of approx. 0.2 eV, if compared to **1F–3F**. Moreover, the two dimethyl-amino substituents on the bpy scaffold are also responsible for the presence of close-lying HOMO–1 and HOMO–2 at only 0.06 and 0.10 eV below the HOMO level (see Figure 2). Such a scenario is very similar to that already observed in the case of [Ir(ppy)$_2$(dmabpy)]$^+$ and [Ir(dfppy)$_2$(dmabpy)]$^+$ complexes, where their HOMO–1 and HOMO–2 are also centered on the dmabpy ancillary ligand and separated by 0.05 eV.[46] Anyway, it should be noted that the HOMO/HOMO–1 gap decreases depending on the nature of the cyclometalating ligands in the order: ppy > dfppy > dfptrz (*i.e.*, 0.40 > 0.15 > 0.10 eV, respectively), due to HOMO stabilization exerted by fluorine substituents and, for **4F**, also because of the presence of the higher-field tetrazole rings.[46]

HOMO stabilization in maximized in complex **5F**, due to the even stronger field exerted by the *tert*-butyl isocyanide ligands, resulting in a stabilization of approx. 0.5 eV with respect to **1F–3F** (Figure 2). Such a phenomenon is already known in literature, both in the case of Ir-ppy or Ir-ptrz complexes, when passing from bpy-type ancillary ligands to isocyanide ones.[28, 34]

As already observed for the fluorine-free Ir-ptrz series, the LUMO of complexes **1F–4F** is always centered on the π* orbitals of the ancillary ligand (Figure 2 and S9). Accordingly, the LUMO energy is strongly affected by the type of ancillary ligand and its related substituents. For instance, in the complexes equipped with a 2,2'-bipyridine ligand, the LUMO energy increases in the order **1F** < **2F** < **4F**, due to the presence of electron-donating substituents on the bpy ancillary ligand of different strength (*i.e.*, none for **1F**, *tert*-butyl for **2F**, and dimethyl-amino for **4F**). Notably, only a minor LUMO stabilization of

approx. 0.08 eV is observed if comparing the Ir-ptrz series with the current Ir-dfptz one, demonstrating that the fluorine substituents on the phenyl-tetrazole cyclometalating ligands exert only a limited effect on the LUMO (Figure S9).

A totally different scenario is observed for complex **5F**, in which the LUMO is located on the tetrazole rings of the cyclometalating ligands, due to the lack of low-energy π^* orbitals in the isocyanide ligands, and appears at much higher energy (Figure 2). The same situation has been already reported for the fluorine-free **5H** analogue,[28] and for other iridium(III) isocyanide complexes.[34, 47]

Electrochemistry. The electrochemical properties of complexes **1F–5F** were investigated by square-wave voltammetry (SWV) and cyclic voltammetry (CV). All the experiments were carried out in room-temperature acetonitrile solutions and reported relative to the Fc⁺/Fc redox couple (see Experimental Section for further details). Redox potentials for all the complexes are collected in Table 2, while the square-wave and cyclic voltammograms are reported in Figure 3 and S10, respectively.
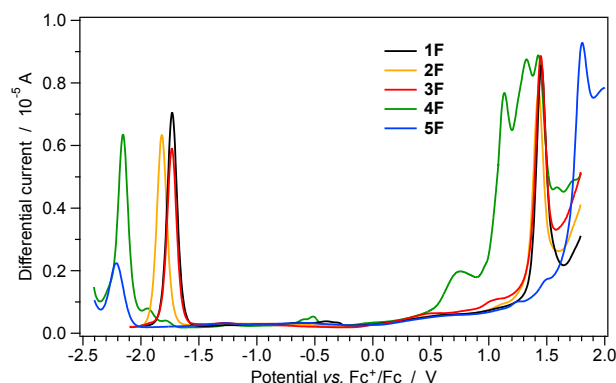

Figure 3. Square-wave voltammograms of complexes **1F–5F** (0.5 mM) in room-temperature acetonitrile solution.

As commonly observed in cationic cyclometalated iridium(III) complexes, the first oxidation process observed for all the investigated complexes can be attributed to the oxidation of the metal center.[16, 18, 28] According to DFT calculations, the oxidation potential of complexes **1F–3F** is found to be virtually identical (*i.e.*, (+1.44 ± 0.01) V), while a substantial anodic shift is observed for **5F**, due to the stronger field exerted by the isocyanide ancillary ligands on the iridium *d* orbitals (*i.e.*, +1.81 V, Table 2).

It is worth noting that the electron-withdrawing fluorine substituents in the dfptrz ligands significantly increase the oxidation potential of the related complexes of approx. 0.28 V, if compared to the analogues of the fluorine-free phenyl-tetrazole series (Table 2).[28] This is a well-known feature for cyclometalated iridium(III) complexes equipped with fluorinated cyclometalating ligands, and it is ascribable to HOMO stabilization (see previous section).[16, 18]

Table 2. Electrochemical Data of 1F–5F in Acetonitrile Solution + 0.1 M TBAPF₆ at 298 K. Data of the fluorine-free series are also reported (1H–5H).[28]

	E_{ox} [a] [V]	E_{red} [a] [V]	ΔE_{redox} [b] [V]
1F	+1.45	−1.73	3.18
2F	+1.43	−1.82	3.25
3F	+1.45	−1.73	3.18
4F	+1.14, +1.33, +1.43	−2.15	3.29
5F	+1.81 *irr.*	−2.21 *irr.*	4.02
1H	+1.16	−1.79	2.95
2H	+1.14	−1.87	3.01
3H	+1.18	−1.77	2.95
5H	+1.57 *irr.*	−2.50 *irr.*	4.07

[a] All potential values are reported vs. the ferrocene/ferrocenium couple, which is used as internal reference. All redox processes are reversible or *quasi*-reversible, unless otherwise stated (*irr.*). [b] $\Delta E_{redox} = E_{ox} − E_{red}$.

The anodic region of complex **4F** shows a more intricate scenario, due to the presence of three oxidations processes occurring at very close potentials (Figure 3 and Table 2). This is due to the presence of the two easily oxidizable dimethyl-amino substituents on the bpy ancillary ligand, which can undergo oxidation readily after the metal center.[46] In order to further confirm that the first oxidation process in complex **4F** can be still attributable to the formal oxidation of iridium(III) to iridium(IV), as already suggested by the frontier molecular orbitals depicted in Figure 2, we carried out a full geometry optimization of the oxidized form of **4F**. The spin-density distribution of the oxidized radical (Figure S11) shows that the hole in mainly located on the iridium ion (*i.e.*, 0.49 e⁻).

As far as the cathodic side is concerned, for complexes **1F–4F**, all reduction processes are fully reversible and monoelectronic, as indicated by a ΔE_p of approx. 0.7 V (Figure S10). Moreover, they are all associated with the reduction of the diamine ancillary ligands (*i.e.*, bpy-type or phen). In excellent agreement with DFT calculation, virtually identical reduction potentials are observed for complexes **1F** and **3F** (*i.e.*, −1.73 V), while the presence of electron-donating substituents on the ancillary ligand, as in **2F** and **4F**, shifts the reduction processes to more negative potentials by 0.09 and 0.42 V, respectively. This kind of cathodic shifts have already been reported for iridium(III) complexes equipped with the same bpy-based ancillary ligands and ppy (or dfppy) cyclometalating ones, and it is attributed to LUMO destabilization.[46] Indeed, our electrochemical shifts compare well with the LUMO destabilization of 0.17 and 0.55 eV calculated for **2F** and **4F**, with respect to the unsubstituted complex **1F** (Figure 2).

Notably, since these reduction processes are centered on the ancillary ligands, the reduction potentials of **1F–3F** display only a minor anodic shift (approx. 0.05 V), if compared to those of their non-fluorinated analogues **1H–3H** (Table 2).[28]

On the contrary, compared to **1F–4F**, the first reduction process in complex **5F** occurs at a lower potential (*i.e.*, −2.21 V) and it is fully irreversible (see Table 2 and Figure S9). This is already known for similar cyclometalated iridium(III) complexes equipped with isocyanide ligands,[28, 33-35, 47] and it is due to the irreversible reduction of the heteroatomic ring of the cyclometalating ligands, as also indicated by DFT calculations (Figure 2). Consequently, the reduction potential of these isocyanide complexes is strongly affected by the nature of the cyclometalating ligands.[33, 34, 47] This is evident from the direct comparison of the reduction potentials of complexes **5F** and **5H** (*i.e.*, −2.21 *vs.* −2.50 V),[28] showing that the fluorine substituents on the phenyl-tetrazole cyclometalating ligands are able to induce a considerable anodic shift of 0.29 V (Table 2).

Photophysical Properties and Excited-State Calculations. All the investigated complexes **1F–5F** are stable in acetonitrile

solutions for months and do not show degradation under standard laboratory conditions. Their room-temperature electronic absorption spectra are reported in Figure 4. In order to allow a comparison, in Figure S12 such spectra are displayed together with those of the their fluorine-free analogues (*i.e.*, **1H–3H** and **5H**).[28]
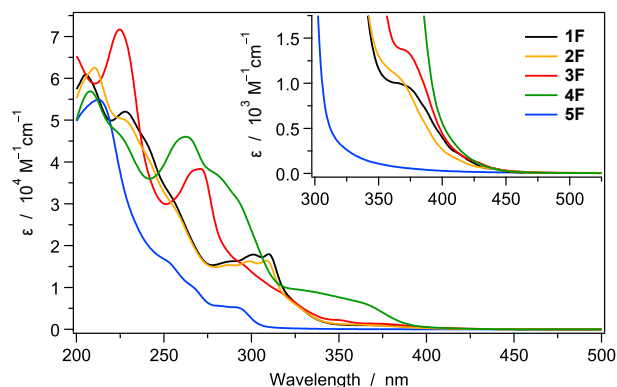

Figure 4. Absorption spectra of complexes **1F–5F** in room-temperature acetonitrile solution; the lower-energy transitions are magnified in the inset. For a comparison with the fluorine-free analogues, see Figure S12.

The main absorption bands in the spectral region 200–300 nm can be assigned to spin-allowed ligand-centered (LC) π–π* transitions involving both the cyclometalating and the ancillary ligands. This can be assessed by comparison with the absorption spectra of the fluorine-free Ir-ptrz analogues, which display virtually identical profiles in this region, with only a minor blue-shift in some absorption peaks (Figure S12).

On the other hand, the weaker and broader bands at longer wavelengths (300−350 nm) are attributed to charge transfer transitions with mixed metal-to-ligand, ligand-to-ligand and intra-ligand charge transfer (MLCT/LLCT/ILCT) character. In fact, a strong blue-shift of approx. 25 nm is observed when passing from the fluorine-free Ir-ptrz series to the current Ir-dfptrz one,[28] as excpected based on HOMO stabilization. Accordingly, the very distinct CT bands observed at 325–350 nm for the fluorine-free complexes **1H–3H** turn out to be blue-shifted in **1F–3F** and largely overlapped with LC absorptions, which do not shift within the two series (Figure S12).

The weak and long tail observed above 350 nm in the spectra of **1F–3F** (inset of Figure 4 and S12) is due to direct spin-forbidden absorption from the singlet ground state (S$_0$) to the lowest triplet excited states of the complexes, enabled by the high spin−orbit coupling constant of the iridium metal core (ζ_{Ir} = 3909 cm^{-1}). The same features are also observed for the fluorine-free **1H–3H** analogues, but with the usual red–shift due to the lack of HOMO stabilization.

On the contrary, in the case of complex **5F**, no absorption features are detected at λ > 300 nm (see inset of Figure 4) because the isocyanide ancillary ligands do not have low-energy π* acceptor orbitals allowing MLCT transitions from the iridium metal center. This is a common feature in cationic iridium(III) complexes with isocyanides.[28, 33-35, 47] Additionally, it is worth noting that the absorption profile of the fluorine-free analogue **5H** (inset of Figure S12) extends up to 325 nm, showing the already mentioned red–shift typical of the complexes lacking the stabilization exerted by the fluorine substituents on the HOMO.[16, 48]

The absorption profile of **4F** displays much more intense bands in the region between 325 and 400 nm, if compared to the other bpy-based complexes of the series (Figure 4). In order to rationalize such experimental finding, we calculated the lowest 50 singlet vertical excitations using a time-dependent DFT (TD-DFT) approach for **4F**. In Figure S13, the calculated singlet vertical excitations are compared with the related experimental spectrum. The transition responsible for such absorption is the S$_0$ → S$_2$ excitation, namely an internal CT transition involving the lone pairs of the dmabpy ancillary ligand, which can occur only in **4F**.

In order to rationalize the emission properties of all the investigated complexes, a combined DFT and TD-DFT approach was adopted and the triplet-state properties of the complexes were investigated in acetonitrile, in order to allow a direct comparison with experimental data. In Tables S2a–e are listed the lowest-energy triplet excitations for all the complexes within the present series (*i.e.*, **1F–5F**), reported in terms of Natural Transition Orbital (NTO) couples.[49] For the sake of comparison, in Tables S2f-h are also reported the lowest-energy triplet transitions of the fluorine-free analogues **1H**, **3H** and **5H**. To provide a compact representation of the triplet-state scenario at the S$_0$ minimum-energy geometries of complexes **1F–5F**, an energy diagram is depicted in Figure 5. The same is also depicted in Figure S14 for **1H**, **3H** and **5H**.
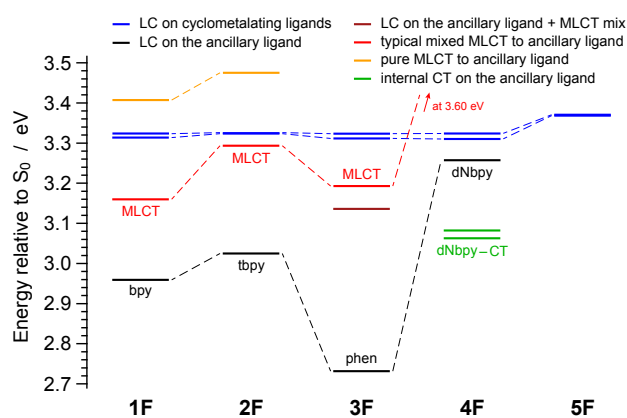
Figure 5. Energy diagram of the lowest-lying triplet states of complexes **1F–5F**, computed in acetonitrile as vertical excitations from the respective ground-state minimum-energy geometries. For further details see Tables S2a–e.

For complexes **1F** and **2F**, the lowest-lying triplet transition (*i.e.*, S$_0$ → T$_1$, estimated at (2.99 ± 0.03) eV, Tables S2a–b) is not associated to a HOMO → LUMO excitation and corresponds to a ligand-centered π–π* transition involving the bpy ancillary ligand, with only a minor MLCT contribution from the iridium *d* orbitals. On the other hand, in both complexes, T$_2$ is the triplet state formally populated by the HOMO → LUMO excitation, which has a strong MLCT component as pointed out in Figure 5. The energy of such state is strongly correlated to the HOMO–LUMO gap (Figure 2) and, as a consequence, it is found at higher energy for complex **2F** with respect to **1F** (*i.e.*, 3.29 *vs.* 3.16 eV, respectively). The next two triplet excited states (*i.e.*, T$_3$ and T$_4$) lie at 3.32 eV above S$_0$ and are associated to transitions mainly involving the two dfptrz cyclometalating ligands (Figure 5).

A similar scenario is also observed for complex **3F**, but a much lower T$_1$, which is again associated to a ^{3}LC π–π* transition involving the ancillary ligand, is observed at 2.73 eV above S$_0$ (Figure 5). Another ^{3}LC π–π* transition on the phen ancillary

ligand is responsible for the S$_0$ → T$_2$ excitation, but with a slightly higher metal contribution (Tables S2c). The ^{3}MLCT state (*i.e.*, T$_3$) is found at 3.19 eV above the ground state, as it could be inferred from the HOMO–LUMO gap of complex **3F** with respect to that of **1F** and **2F**. On the contrary, the ^{3}LC states centered on the cyclometallating ligands (*i.e.*, T$_4$ and T$_5$) are virtually located at the same energy as in **1F** and **2F**.

Drastic differences are found for **4F**. In this complex, T$_1$ and T$_2$ are nearly degenerate (*i.e.*, approx. 3.07 eV above S$_0$) and are associated to an internal CT transition within the dmabpy ancillary ligand, which can be seen as the excitation of one electron from the amine lone pairs to the π* orbitals on the bpy core (Figure 5 and Table S2d). These CT states are well separated from T$_3$, which has the same topology of the T$_1$ state of **1F** and **2F** (*i.e.*, the ^{3}LC π–π* state on the bpy ancillary ligand) and is located approx. 0.2 eV higher in energy. Notably, due to the strong electron donating effect of the dimethyl-amino substituents, the MLCT state (*i.e.*, T$_2$ state in **1F** and **2F**) is extremely destabilized in complex **4F** and it is located at 3.60 eV above S$_0$, which is even higher in energy with respect to the ^{3}LC states centered on the cyclometalated ligands (*i.e.*, T$_4$ and T$_5$, Figure 5 and Table S2d).

In the case of **5F**, the lowest-lying triplet excited states are virtually degenerate and centered on the dftrz cyclometalating ligands at 3.37 eV above S$_0$ (Table S2e). A virtually identical scenario is observed for **5H**, where T$_1$ and T$_2$ are centered on the fluorine-free ptrz cyclometalating ligands at 3.23 eV above the ground state (Table S2h). As a consequence, a very similar ligand-centered emission is expected for both these isocyanide complexes, with that of **5F** being blue-shifted compared to **5H**.

The emission spectra of complexes **1F–5F** in diluted acetonitrile solution are shown in Figure 6, where both the room-temperature (full lines) and the 77 K spectra (dashed) are gathered to allow an easy comparison. The luminescence properties and photophysical parameters are summarized in Table 3. With respect to the fluorine-free series, complexes **1F–5F** display a much bluer emission as shown in the CIE-1931 chromaticity diagram in Figure S15.

As predicted by TD-DFT calculations, all the investigated complexes (except **4F**) emit from strongly LC triplet states, as suggested by: (i) vibrationally resolved emission spectra both at 298 and 77 K; (ii) virtually no shift on passing from room-temperature solution to frozen matrix at 77 K. (Figure 6).

On the contrary, in the case of **4F**, a broad and unstructured emission band is recorded at 298 K, which becomes more structured and undergoes a slight blue-shift as the temperature decreases to 77 K. This can be an indication of a partial CT nature of the emissive state, in agreement with TD-DFT calculations.

By comparison with the fluorine-free Ir-ptrz series, it is possible to assess that the ^{3}LC emissive state of complexes **1F–3F** is centered on the ancillary ligand (*i.e.*, bpy-type or phen) since the 77 K spectra of the fluorine-free analogues **1H–3H** are virtually mutually superimposable to the ones of **1F–3F**, without being perturbed by the electron-withdrawing substituents on the cyclometalated ligands (Figure S16).

Table 3. Luminescence Properties and Photophysical Parameters of Complexes 1F–5F

	CH$_3$CN oxygen-free solution, 298 K					CH$_3$CN rigid matrix, 77 K		1% PMMA matrix, 298 K		
	$\lambda_{em}{}^a$ [nm]	PLQY ^{a} [%]	τ^b [µs]	$k_r{}^c$ [10^5 s^{-1}]	$k_{nr}{}^d$ [10^4 s^{-1}]	$\lambda_{em}{}^a$ [nm]	τ^b [µs]	$\lambda_{em}{}^e$ [nm]	PLQY^e [%]	τ^b [µs]
1F	449, 480, 503^{sh}	75.9	4.11	1.85	5.86	446, 478, 508, 540	8.02	446, 477, 506, 542^{sh}	71.9	3.89
2F	451, 480, 505^{sh}	57.6	4.90	1.17	8.66	443, 472, 502, 538	8.93	448, 476, 502, 540^{sh}	63.7	6.39
3F	459, 490, 520^{sh}	56.3	43.8	0.13	1.00	457, 489, 525, 562	71.9	458, 489, 522, 563^{sh}	40.1	46.1
4F	500	40.2	10.3	0.39	5.79	468, 490	20.7	498	24.6	11.9
5F	386, 407, 428	0.6	1.21	0.05	82.1	383, 407, 434	117	384, 407, 431	1.1	0.97

^{a} λ_{exc} = 290 nm. ^{b} λ_{exc} = 280 and/or 370 nm. ^{c} Radiative constant: k_r = PLQY/τ. ^{d} Non-radiative constant: k_{nr} = 1/τ – k_r. ^{e} λ_{exc} = 370 nm.
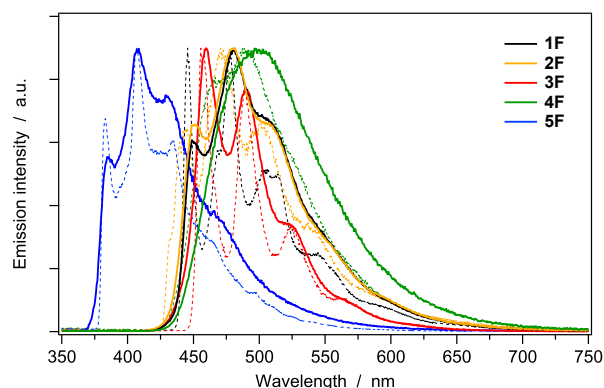
Figure 6. Normalized emission spectra of complexes **1F–5F** in acetonitrile at 298 K (thick full) and at 77 K (thin dotted).

On the other hand, the emission of the isocyanide complex **5F** is considerably blue-shifted compared to **1F–3F**, since it arises from a ^{3}LC state centered on the cyclometalating moieties and not from the one centered on the ancillary ligands. This is typically observed in cyclometalated iridium(III) complexes equipped with isocyanide ligands.[28, 34] This attribution is further confirmed by the blue-shift of approx. 15 nm (*i.e.*, 0.10 eV) observed both at 77 K and at room temperature (Figures S16 and S17, respectively), when passing from the fluorine-free complex **5H**, having ptrz cyclometalating ligands, to the fluorinated **5F** analogue, equipped with dfptrz ones.[28]

Such a picture is further validated by spin-unrestricted DFT calculations, carried out to optimize the lowest triplet states of all the complexes. As expected, the T_1 spin-density distribution in isocyanide complexes is mainly localized on the cyclometalated ligands and its emission energy is calculated at 2.87 and 2.73 eV, for **5F** and **5H**, respectively (see Figure S18). This prediction is in line with the mean-photon energy of 2.90 and 2.79 eV, calculated from experimental data (Figure 6 and S17).

In complex **4F**, upon relaxation, the emissive state preserves the internal CT character on the dmabpy ancillary ligand (as indicated by TD-DFT calculations, Table S2d), but it becomes more localized on only one lone pair of the dmabpy ligand, allowing a greater stabilization due to a considerable geometrical rearrangement (Figure S19). As a consequence, T_1 is only 2.47 eV above S_0, which is in excellent agreement with the experimental emission maximum of 500 nm (*i.e.*, 2.48 eV, see Table 3).

A more complicated excited-state scenario is observed for **1F–3F**, due to the interplay between the ^{3}MLCT state and the ^{3}LC one centered on the ancillary ligand. Such a situation was already seen for the fluorine-free Ir-ptrz series, and it was responsible for the experimentally observed emissive-state switching from ^{3}MLCT to ^{3}LC, when passing from room-temperature solution to frozen matrix at 77 K.[28] On the other hand, in the case of the present Ir-dfptrz series, the ^{3}LC state is always found to be the lowest triplet for **1F–3F** (Figure S20). In fact, compared to the fluorine-free analogues **1H–3H**, the energy of the ^{3}MLCT state of **1F–3F** is so up in energy, that, despite the larger relaxation typical of ^{3}MLCT, the ^{3}LC state on the ancillary ligand remains the lowest one even after excited-state relaxation. This scenario is sketched for the phen-based complexes **3H** and **3F** in Figure 7.
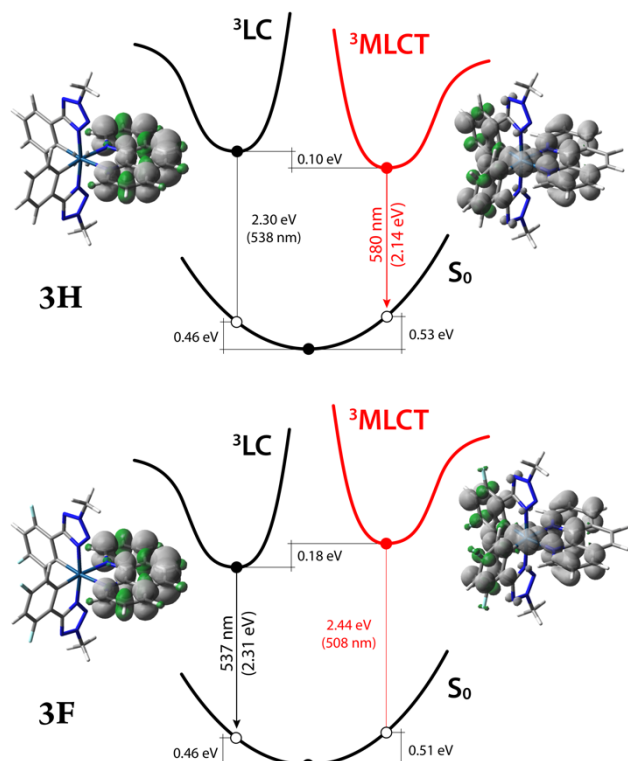

Figure 7. Schematic energy diagram for **3H** (top) and **3F** (bottom) showing the adiabatic energy differences between S_0 and the lowest

triplet states (*i.e.*, ^{3}MLCT and ^{3}LC). The estimated emission energies are also reported. The unpaired-electron spin-density surfaces calculated at the fully-relaxed triplet-state minima are also depicted (isosurfaces: 0.002 e bohr^{-3}). The energy scale is not proportional to allow a better visibility.

As far as photoluminescence quantum yields are concerned, **1F–4F** are bright emitters (PLQY ≈ 60%, Table 3) and only the isocyanide complex **5F** displays a quantum yield below 1%, due to extremely fast non-radiative deactivation processes (*i.e.*, high k_{nr} value, Table 3) combined with the low radiative rate constant of the ^{3}LC states, typically observed for iridium(III) isocyanide complexes.[33-35, 47] Such a finding was also observed for the fluorine-free analogue **5H** (Table S3).[28]

Emission lifetimes of **1F–3F** are much longer compared to **1H–3H**, despite PLQYs are comparable (Table 3 and S3). This results in lower radiative rate constants, as typically observed when passing from predominantly ^{3}MLCT states to ^{3}LC ones.[16] This effect is extremely evident in the case of the complexes equipped with the phen ancillary ligand, in which the k_r constant decreases more than 30 times (*i.e.*, from 4.22 to 0.13 · 10^5 s^{-1} in **3H** and **3F** respectively, Table 3 and S3). On the other hand, in the case of the bpy-based complexes **1F–2F**, the k_r constants decreases approximately only by a factor of three, compared to the analogues **1H–2H** (Table 3 and S3). Such reduction in the k_r value is one order of magnitude less pronounced than in the case of phen-based complexes.

This can be tentatively explained due to the much lower energy difference between the ^{3}MLCT and lowest-lying ^{3}LC state centered on the ancillary ligand (*i.e.*, 0.04 *vs.* 0.18 eV in **1F** and **3F**, respectively), which can allow a thermal equilibration between these two states and shorten the emission lifetimes of **1F–2F**. Moreover, it should be stressed that the ^{3}LC states of **1F–2F** have some degree of contribution from the iridium *d* orbitals to the triplet spin densities, while the ^{3}LC state of **3F** has none (Figure S20).

For the sake of completeness, the emission properties of the complexes were also investigated in the solid state, that is, dispersed in a poly(methyl-methacrylate) (PMMA) matrix at a concentration of 1% by weight. The corresponding emission spectra are reported in Figure S21 and the photophysical parameters are gathered in Table 3. No substantial differences have been observed compared to the oxygen-free acetonitrile solution.

■ CONCLUSIONS

A new family of cationic iridium(III) complexes has been synthesized and fully characterized. The strategy for ligand design aimed at making robust tetrazole-based systems with enhanced excited-state energy turned out to be successful. The insertion of two fluorine atoms on the six-membered ring of the phenyl tetrazole cyclometallating units increases the ligand field, widens the HOMO–LUMO gap and pushes the luminescence bands towards the blue region. The electrochemical and photophysical behavior of the five compounds has been rationalized with the essential support of density functional theory. The level of thorough understanding of the electronic properties achievable for cyclometalated iridium(III) complexes suggests that they can be virtually tailored by design, so that materials with subtly tuned optical and electrochemical properties can be made readily available, whenever an efficient synthetic route is established.

Thanks to their accessibility, robustness and good solubility, complexes **1F**–**4F** can serve as blue emitters in several applications. On the other hand, we previously demonstrated that non fluorinated analogues of these compounds are excellent photoredox catalysts.[32] The higher excited state energy (*e.g.*, 2.54 *vs.* 2.24 eV for **3F** and **3H**, respectively), combined with favorable oxidation potentials (*e.g.*, +1.45 *vs.* +1.18 V for **3F** and **3H**), can make the compounds of the present series even superior, for this specific application (with excited-state oxidation potential as high as +0.81 eV for **3F**). We are currently working to develop this unexplored potential.

■ EXPERIMENTAL SECTION

General Information. Analytical grade solvents and commercially available reagents were used as received unless otherwise stated. Chromatographic purifications were performed using 70−230 mesh silica gel or using aluminum oxide. ^{1}H, ^{19}F, and ^{13}C NMR spectra were recorded on Varian Inova (300 and 600 MHz for ^{1}H) and Varian Mercury (400 MHz for ^{1}H) spectrometers. Chemical shifts (δ) are reported in ppm relative to residual solvent signals for ^{1}H and ^{13}C NMR (^{1}H NMR: 7.26 ppm for CDCl$_3$, 1.94 ppm for CD$_3$CN, 3.34 ppm for CD$_3$OD, 2.05 ppm for (CD$_3$)$_2$CO, 2.50 ppm for (CD$_3$)$_2$SO, 5.33 ppm for CD$_2$Cl$_2$; ^{13}C NMR: 77.0 ppm for CDCl$_3$, 1.32 ppm for CD$_3$CN, 48.9 ppm for CD$_3$OD, 29.8 ppm for (CD$_3$)$_2$CO, 39.5 ppm for (CD$_3$)$_2$SO, 53.5 ppm for CD$_2$Cl$_2$). ^{19}F NMR spectra were recorded at 376.25 MHz or at 564.3 MHz using trichlorofluoromethane as an external standard. ^{13}C NMR spectra were acquired with ^{1}H broadband decoupled mode. Coupling constants are given in Hz. The high-resolution mass spectra (HRMS) were obtained with an ESI-QTOF (Agilent Technologies, model G6520A) instrument, and the m/z values are referred to the monoisotopic mass. ESI-MS analyses were performed by direct injection of acetonitrile solutions of the compounds using a WATERS ZQ 4000 mass spectrometer.

Caution: Although we experienced no difficulties in handling these nitrogen rich compounds, small scale and best safety practices are strongly encouraged.

Preparation of Ligand III.

Synthesis of 5-(2,4-difluoro-phenyl)-1H-tetrazole (**II**). NaN$_3$ (546.0 mg, 8.4 mmol) was dissolved in H$_2$O (10 mL), then ZnCl$_2$ (1.14 g, 8.4 mmol) and CH$_3$COOH (1 mL) were added. The solution was stirred for 10 minutes. Then 2,4-difluorobenzonitrile (**I**) (1.17 g, 8.4 mmol) was added and the resulting mixture was refluxed for 6 hours. After this time the solution was cooled and HCl 1M (1 mL) was added. The resulting solid was filtered and washed with cold water. Product **II** was isolated in 80% yield (1.23 g) and used in the next step without further purifications. ^{1}H NMR ((CD$_3$)$_2$SO, 300 MHz) δ 7.88 (dt, J_1 = 6.9 Hz, J_2 = 8.6 Hz 1H), 7.29 (ddd, J_1 = 2.6 Hz, J_2 = 9.5 Hz, J_3 = 10.7 Hz, 1H), 7.11 (ddt, J_1 = 0.9 Hz, J_2 = 2.6 Hz, J_3 = 8.6 Hz, 1H). ^{13}C NMR ((CD$_3$)$_2$SO, 100 MHz) δ 162.6 (C, dd, J_{CF} = 12.6 Hz, J_{CF} = 225.2 Hz), 159.2 (C, dd, J_{CF} = 12.9 Hz, J_{CF} = 229.9 Hz),156.5 (C, d, J_{CF} = 6 Hz), 131.5 (CH, dd, J_{CF} = 4.8 Hz, J_{CF} = 10.1 Hz), 114.4 (C, d, J_{CF} = 3.7 Hz), 111.7 (CH, dd, J_{CF} = 3.8 Hz, J_{CF} = 21.6 Hz), 104.6 (CH, t, J_{CF} = 25.9 Hz). ^{19}F NMR ((CD$_3$)$_2$SO, 376 MHz) δ -109.3 (quint, J = 8.5 Hz, 1F), -108.1 (q, J = 9.4 Hz, 1F).

Synthesis of 5-(2,4-difluoro-phenyl)-2-methyl-2H-tetrazole (**III**). 5-(2,4-difluorophenyl)-1*H*-tetrazole (**II**) (746.2 mg, 4.1 mmol) was dissolved in a mixture of acetone/water 3:1 (16 mL). Then NaOH (330.0 mg, 8.2 mmol) and MeI (510 μL, 8.2 mmol)

were added and the resulting mixture was refluxed for 2 hours. After this time solvent was evaporated. Water (30 mL) was added and the mixture was extracted with DCM (4 x 15 mL). The collected organic phase was washed with water (30 mL) and brine (30 mL), dried over Na$_2$SO$_4$ and concentrated. The crude was purified on silica gel flash chromatography using a mixture of EP/DCM (50:50) and then DCM/methanol (95:5) to give product **III** in 40% yield (305.4 mg). ^{1}H NMR (CDCl$_3$, 400 MHz) δ 8.14 (dt, J_1 = 6.4 Hz, J_2 = 8.0 Hz, 1H), 7.06-6.97 (m, 2H), 4.44 (s, 3H). ^{13}C NMR (CDCl$_3$, 100 MHz) δ 163.8 (C, dd, J_{CF} = 12 Hz, J_{CF} = 254 Hz), 160.5 (C, d, J_{CF} = 6 Hz), 160.3 (C, dd, J_{CF} = 12 Hz, J_{CF} = 254 Hz), 130.9 (CH, dd, J_{CF} = 4 Hz, J_{CF} = 10 Hz), 111.9 (C, d, J_{CF} = 4 Hz), 111.8 (CH, dd, J_{CF} = 4 Hz, J_{CF} = 24 Hz), 104.8 (CH, t, J_{CF} = 24 Hz), 39.4 (CH$_3$). ^{19}F NMR (CDCl$_3$, 400 MHz) δ -107.4 (q, J = 8.0 Hz, 1F), -106.2 (quint, J = 8.0 Hz, 1F).

General Procedures for the Synthesis of Complexes 1F–5F.

5-(2,4-difluorophenyl)-2-methyl-2*H*-tetrazole (**III**) (3 equiv, 59.2 mg, 0.3 mmol) was dissolved in a mixture of 2-ethoxyethanol/water 3:1 (2.0 mL) and the solution was degassed with N$_2$ for 20 minutes. Then, IrCl$_3$×H$_2$O (1 equiv, 30.0 mg, 0.1 mmol) was added and the resulting mixture was refluxed for 24 hours in N$_2$ atmosphere. After this time, water (1 mL) was added and the resulting precipitate was collected and washed with additional water (1 mL). The solid was then dissolved in DCM (8.0 mL) and AgPF$_6$ (2 equiv, 50.6 mg, 0.2 mmol,) was added. The resulting mixture was refluxed for 6 hours and the former precipitate was filtered off. The solvent was then evaporated and the solid added to the proper ancillary ligand (3 equiv,0.3 mmol) dissolved in a mixture of CH$_2$Cl$_2$/ethanol 3:1 (4 mL). The resulting solution was stirred for 24 hours at room temperature. The solvent was evaporated, and the crude was purified on Al$_2$O$_3$ gel flash chromatography using a mixture of CH$_2$Cl$_2$/methanol (95:5) to give the desired products.

[Ir(dfptrz)$_2$(bpy)]$^+$PF$_6^-$ (1F). 47.7 mg, 0.054 mmol, yield = 54%. ^{1}H NMR (CDCl$_3$, 400 MHz) δ 9.54 (d, J = 8.1 Hz, 2H), 8.33 (d, J = 7.5 Hz, 2H), 7.95 (d, J = 5.3 Hz, 2H), 7.47 (t, J = 6.65 Hz, 2H), 6.64 (td, J_T = 9.7 Hz, J_D = 2.2 Hz, 2H), 5.71 (dd, J = 8.4, 2.1 Hz, 2H), 4.42 (s, 6H). ^{13}C NMR (CDCl$_3$, 100 MHz) δ 171.5 (C, d, J_{CF} = 6 Hz), 164.9 (C, dd, J_{CF} = 12 Hz, J_{CF} = 254 Hz), 159.5 (C, dd, J_{CF} = 12 Hz, J_{CF} = 254 Hz), 156.8 (C), 150.6 (CH), 149.7 (C, d, J_{CF} = 6 Hz), 141.2 (CH), 127.7 (CH), 127.1 (CH), 115.3 (CH, dd, J_{CF} = 4 Hz, J_{CF} = 22 Hz), 113.5 (C, dd, J_{CF} = 4 Hz, J_{CF} = 14 Hz), 99.8 (CH, dd, J_{CF} = 24 Hz, J_{CF} = 28 Hz), 42.1 (CH$_3$). ^{19}F NMR (CDCl$_3$, 400 MHz) δ -106.8 (t, J = 10.5 Hz, 2F), -102.9 (q, J = 9.5 Hz, 2F), -73.4 (d, J = 712.5 Hz, 6F). ESI-MS: 739 [M$^+$], 145 [M$^-$]. HRMS (ESI-QTOF) ([M]$^+$): m/z calcd for C$_{26}$H$_{18}$F$_4$IrN$_{10}^+$: 737.1252; found: 737.1224.

[Ir(dfptrz)$_2$(dtbbpy)]$^+$PF$_6^-$ (2F). 52.8 mg, 0.053 mmol, yield = 53%. ^{1}H NMR (CDCl$_3$, 400 MHz) δ 8.67 (bs, 2H), 7.90 (d, J = 5.9 Hz, 2H), 7.43 (dd, J = 5.9, 1.8 Hz, 2H), 6.62 (td, J_T = 9.5 Hz, J_D = 2.0 Hz, 2H), 5.60 (dd, J = 8.3, 2.1 Hz, 2H), 4.45 (s, 6H), 1.45 (s, 18H). ^{13}C NMR (CDCl$_3$, 100 MHz) δ 171.3 (C, d, J_{CF} = 6 Hz), 164.9 (C, dd, J_{CF} = 12 Hz, J_{CF} = 254 Hz), 164.8 (C), 159.5 (C, dd, J_{CF} = 12 Hz, J_{CF} = 254 Hz), 156.3 (C), 150.7 (CH), 150.2 (C, d, J_{CF} = 6 Hz), 125.2 (CH), 121.3 (CH), 115.3 (CH, dd, J_{CF} = 4 Hz, J_{CF} = 22 Hz), 113.7 (C, dd, J_{CF} = 4 Hz, J_{CF} = 14 Hz), 99.6 (CH, dd, J_{CF} = 24 Hz, J_{CF} = 28 Hz), 42.0 (CH$_3$), 35.8 (C), 30.2 (CH$_3$). ^{19}F NMR (CDCl$_3$, 400 MHz) δ -107.3 (t, J = 10.5 Hz, 2F), -103.6 (q, J = 9.5 Hz, 2F), -73.4 (d, J = 712.5 Hz, 6F). ESI-MS: 851 [M$^+$], 145 [M$^-$]. HRMS (ESI-QTOF)

([M]+): m/z calcd for $C_{34}H_{34}F_4IrN_{10}^+$: 849.2504; found: 849.2500.

[Ir(dfptrz)₂(phen)]⁺PF₆⁻ (3F). 42.7 mg, 0.047 mmol, yield = 47%. ^{1}H NMR (CD₂Cl₂, 400 MHz) δ 8.70 (dd, J = 8.1, 0.9 Hz, 2H), 8.43 (dd, J = 5.1, 1.2 Hz, 2H), 8.22 (s, 2H), 7.88 (dd, J = 8.3, 5.0 Hz, 2H), 6.75 (td, J_T = 9.8 Hz, J_D = 2.3 Hz, 2H), 5.95 (dd, J = 8.3, 2.1 Hz, 2H), 4.30 (s, 6H). ^{13}C NMR (CD₂Cl₂, 100 MHz) δ 171.5 (C, d, J_{CF} = 6 Hz), 165.0 (C, dd, J_{CF} = 259.3 Hz, J_{CF} = 12 Hz), 159.5 (C, dd, J_{CF} = 261.8 Hz, J_{CF} = 12 Hz), 152.2 (C), 148.6 (C, d, J_{CF} = 6 Hz), 147.5 (C), 139.4 (CH), 131.4 (CH), 128.4 (CH), 126.3 (CH), 115.7 (CH, dd, J_{CF} = 18.8 Hz, J_{CF} = 4 Hz), 114.0 (C, dd, J_{CF} = 9.7 Hz, J_{CF} = 3 Hz), 99.8 (CH, dd, J_{CF} = 28 Hz, J_{CF} = 24 Hz), 41.9 (CH₃). ^{19}F NMR (CDCl₃, 400 MHz) δ -107.7 (t, J = 10.6 Hz, 2F), -104.2 (q, J = 9.5 Hz, 2F), -73.5 (d, J = 711.4 Hz, 6F). ESI-MS: 763 [M⁺], 145 [M⁻]. HRMS (ESI-QTOF) ([M]⁺): m/z calcd for $C_{28}H_{18}F_4IrN_{10}^+$: 761.1252; found: 761.1266.

[Ir(dfptrz)₂(dmabpy)]⁺PF₆⁻ (4F). 4,4'-bis (dimethyla-mino)-2,2'-bipyridine ancillary ligand was synthesized following a previously reported procedure with slight modifications.[50] In order to obtain complex **4F** with a higher degree of purity, after the column chromatography, the complex was crystallized from a dichloromethane/diethyl ether mixture. After several failed attempts, in order to facilitate this process, and to obtain crystals also suitable for X-ray analysis, the counterion was changed using an excess of ammonium trifluoroacetate. 49.5 mg, 0.053 mmol, yield = 53%. ^{1}H NMR (CDCl₃, 400 MHz) δ 8.26 (d, J = 2.8 Hz, 2H), 7.34 (d, J = 6.7 Hz, 2H), 6.59 (td, J_T = 9.5 Hz, J_D = 2.3 Hz, 2H), 6.33 (dd, J = 6.9, 2.8 Hz, 2H), 5.74 (dd, J = 8.5, 2.3 Hz, 2H), 4.44 (s, 6H), 3.28 (bs, 12H). ^{13}C NMR (CDCl₃, 100 MHz) δ 171.7 (C, d, J_{CF} = 6 Hz), 170.3 (CO, q, J_{CF} = 21 Hz), 164.7 (C, dd, J_{CF} = 258 Hz, J_{CF} = 12 Hz), 159.4 (C, dd, J_{CF} = 262.7 Hz, J_{CF} = 12 Hz), 156.8 (C), 155.4 (C), 153.1 (C, d, J_{CF} = 6 Hz), 149.0 (CH), 120 (CF₃, q, J_{CF} = 256 Hz),115.4 (CH, dd, J_{CF} = 4 Hz, J_{CF} = 22 Hz), 113.6 (C, dd, J_{CF} = 4 Hz, J_{CF} = 14 Hz), 108.0 (CH), 107.8 (CH), 98.8 (CH, dd, J_{CF} = 24 Hz, J_{CF} = 28 Hz), 41.8 (CH₃), 40.2 (CH₃). ^{19}F NMR (CDCl₃, 400 MHz) δ -112.9 (t, J = 10.0 Hz, 2F), -109.3 (q, J = 9.1 Hz, 2F), -79.7 (s, 3F). HRMS (ESI-QTOF) ([M]⁺): m/z calcd for $C_{30}H_{28}F_4IrN_{12}^+$: 823.2096; found: 823.2084.

[Ir(dfptrz)₂(CNtBu)₂]⁺PF₆⁻ (5F). 41.1 mg, 0.046 mmol, yield = 46%. ^{1}H NMR (CDCl₃, 400 MHz) δ 6.57 (td, J_T = 9.6 Hz, J_D = 2.3 Hz 2H), 5.55 (dd, J = 8.0, 2.2 Hz, 2H), 4.72 (s, 6H), 1.48 (s, 18H). ^{13}C NMR (CDCl3, 100 MHz) δ 171.3 (C, d, J_{CF} = 6 Hz), 164.7 (C, dd, J_{CF} = 258 Hz, JC-F = 12 Hz), 162.7 (C), 159.4 (C, dd, J_{CF} = 263 Hz, J_{CF} = 12 Hz), 152.8 (C, d, J_{CF} = 6 Hz), 114.1 (CH, dd, J_{CF} = 19 Hz, J_{CF} = 4 Hz), 113.0 (C, dd, J_{CF} = 10 Hz, J_{CF} = 4 Hz), 100.4 (CH, dd, J_{CF} = 27 Hz, J_{CF} = 22 Hz), 59.4 (C), 42.4 (CH₃), 30.1(CH₃). ^{19}F NMR (CDCl₃, 400 MHz) δ -107.8 (t, J = 10.1 Hz, 2F), -103.6 (q, J = 9.6 Hz, 2F), -73.3 (d, J = 711.9 Hz, 6F). ESI-MS: 749 [M⁺], 145 [M⁻]. HRMS (ESI-QTOF) ([M]⁺): m/z calcd for $C_{26}H_{28}F_4IrN_{10}^+$: 747.2035; found: 747.2016.

Electrochemical characterization. Voltammetric experiments were performed using a Metrohm AutoLab PGSTAT 302N electrochemical work-station in combination with the NOVA 2.0 software package. All the measurements were carried out at room temperature in acetonitrile solutions with a sample concentration approximately 0.5 mM and using 0.1 M tetrabutylammonium hexafluorophosphate (electrochemical grade, TBAPF₆) as the supporting electrolyte. Oxygen was removed from the solutions by bubbling argon. All the experiments were carried out using a three-electrode setup (Bi-oLogic VC-4 cell, volume range: 1−3 mL) using a platinum or a glassy carbon working electrode (both having an active surface disk of 1.6 mm in diameter), the Ag/AgNO₃ redox couple (0.01 M in acetonitrile, with 0.1 M TBAClO₄ supporting electrolyte) as the reference electrode and a platinum wire as the counter electrode. At the end of each measurement, ferrocene was added as the internal reference. Cyclic voltammograms (CV) were recorded at different scan rates, from 100 to 1000 mV s⁻¹. Osteryoung square-wave voltammograms (OSWV) were recorded with scan rate of 125 mV s⁻¹, a SW amplitude of ±20 mV, and a frequency of 25 Hz.

Photophysics. The spectroscopic investigations were carried out in spectrofluorimetric grade acetonitrile. The absorption spectra were recorded with a PerkinElmer Lambda 950 spectrophotometer. For the photoluminescence experiments, the sample solutions were placed in fluorimetric Suprasil quartz cuvettes (10.00 mm) and dissolved oxygen was removed by bubbling argon for 30 min. The uncorrected emission spectra were obtained with an Edinburgh Instruments FLS920 spectrometer equipped with a Peltier-cooled Hamamatsu R928 photomultiplier tube (PMT, spectral window: 185−850 nm). An Osram XBO xenon arc lamp (450 W) was used as the excitation light source. The corrected spectra were acquired by means of a calibration curve, obtained by using an Ocean Optics deuterium–halogen calibrated lamp (DH-3plus-CAL-EXT). The photoluminescence quantum yields (PLQYs) in solution were obtained from the corrected spectra on a wavelength scale (nm) and measured according to the approach described by Demas and Crosby,[51] using an air-equilibrated water solution of quinine sulfate in 1 N H₂SO₄ as reference (PLQY = 0.546).[52] The emission lifetimes (τ) were measured through the time-correlated single photon counting (TCSPC) technique using an HORIBA Jobin Yvon IBH FluoroHub controlling a spectrometer equipped with a pulsed SpectraLED (λ_{exc} = 373 nm) or NanoLED (λ_{exc} = 280 nm) as the excitation source and a red-sensitive Hamamatsu R-3237-01 PMT (185−850 nm) as the detector. The analysis of the luminescence decay profiles was accomplished with the DAS6 Decay Analysis Software provided by the manufacturer, and the quality of the fit was assessed with the χ^2 value close to unity and with the residuals regularly distributed along the time axis. To record the 77 K luminescence spectra, samples were put in quartz tubes (2 mm inner diameter) and inserted into a special quartz Dewar flask filled with liquid nitrogen. The poly(methyl methacrylate) (PMMA) films containing 1% (w/w) of the complex were obtained by drop casting and the thickness of the films was not controlled. Solid-state PLQY values were calculated by corrected emission spectra obtained from an Edinburgh FLS920 spectrometer equipped with a barium sulfate- coated integrating sphere (diameter of 4 in.) following the procedure described by Würth et al.[53] Experimental uncertainties are estimated to be ±8% for τ determinations, ± 10% for PLQYs, ± 2 nm and ±5 nm for absorption and emission peaks, respectively.

Computational details. Density functional theory (DFT) calculations were carried out using the B.01 revision of the Gaussian 16 program package[54] in combination with the M06 global-hybrid meta-GGA exchange-correlation functional.[39, 40] The fully relativistic Stuttgart/Cologne energy-consistent pseudopotential with multielectron fit was used to replace the first 60 inner-core electrons of the iridium metal center (i.e., ECP60MDF) and was combined with the associated triple-ζ

basis set (*i.e.*, cc-pVTZ-PP basis).[42] On the other hand, the Pople 6-31G(d,p) basis was adopted for all other atoms.[41]

All the reported complexes were fully optimized without symmetry constraints, using a time-independent DFT approach, in their ground state (S_0) and lowest triplet states; all the optimization procedures were performed using the polarizable continuum model (PCM) to simulate acetonitrile solvation effects.[43-45] Frequency calculations were always used to confirm that every stationary point found by geometry optimizations was actually a minimum on the corresponding potential-energy surface (no imaginary frequencies). To investigate the nature of the emitting states, geometry optimizations and frequency calculations were performed at the spin-unrestricted UM06 level of theory (imposing a spin multiplicity of 3), using the S_0 minimum-energy geometry as initial guess or previously optimized triplet states at the TD-DFT level (see below). The emission energy from the lowest triplet excited states was estimated by subtracting the SCF energy of the emitting state (T_n) in its minimum conformation from that of the singlet ground state having the same geometry and equilibrium solvation of T_n.

Time-dependent DFT calculations (TD-DFT),[55-57] carried out at the same level of theory used for geometry optimizations, were used to calculate the first 25 triplet excitations and their nature was assessed by the help of Natural Transition Orbital (NTO) analysis.[49] Some selected states of interest were also optimized at the TD-DFT level of theory.

All the pictures showing molecular geometries, orbitals and spin-density surfaces were created using GaussView 6.[58] The structural overlaps between different structures were obtained thanks to the VMD program,[59] by minimizing the root-mean-square deviation (RMSD) of all or selected atomic positions.

■ ASSOCIATED CONTENT

Supporting Information

NMR spectra, crystal structures and crystallographic data, electrochemical and photophysical data, DFT tables and figures (PDF). X-ray crystallographic data in CIF format (CIF). This material is available free of charge on the ACS Publications website.

■ AUTHOR INFORMATION

Corresponding Author

* (F.M.) E-mail: filippo.monti@isof.cnr.it
* (A.B.) E-mail: andrea.baschieri@univaq.it

ORCID

Andrea Baschieri: 0000-0002-2108-8190

Letizia Sambri: 0000-0003-1823-9872

Andrea Mazzanti: 0000-0003-1819-8863

Armando Carlone: 0000-0003-2983-6445

Filippo Monti: 0000-0002-9806-1957

Nicola Armaroli: 0000-0001-8599-0901

Notes

The authors declare no competing financial interest.

■ ACKNOWLEDGMENT

■ REFERENCES

1. Flamigni, L.; Barbieri, A.; Sabatini, C.; Ventura, B.; Barigelletti, F., Photochemistry and Photophysics of Coordination Compounds: Iridium. In *Photochemistry and Photophysics of Coordination Compounds II*, 2007; pp 143-203.

2. Lamansky, S.; Djurovich, P.; Murphy, D.; Abdel-Razzaq, F.; Lee, H. E.; Adachi, C.; Burrows, P. E.; Forrest, S. R.; Thompson, M. E., Highly Phosphorescent Bis-Cyclometalated Iridium Complexes: Synthesis, Photophysical Characterization, and Use in Organic Light Emitting Diodes. *J Am Chem Soc* **2001,** 123, (18), 4304-12.

3. You, Y.; Park, S. Y., Inter-Ligand Energy Transfer and Related Emission Change in the Cyclometalated Heteroleptic Iridium Complex: Facile and Efficient Color Tuning over the Whole Visible Range by the Ancillary Ligand Structure. *J Am Chem Soc* **2005,** 127, (36), 12438-9.

4. Chi, Y.; Chou, P. T., Transition-Metal Phosphors with Cyclometalating Ligands: Fundamentals and Applications. *Chem Soc Rev* **2010,** 39, (2), 638-55.

5. Yersin, H.; Rausch, A. F.; Czerwieniec, R.; Hofbeck, T.; Fischer, T., The Triplet State of Organo-Transition Metal Compounds. Triplet Harvesting and Singlet Harvesting for Efficient Oleds. *Coordination Chemistry Reviews* **2011,** 255, (21-22), 2622-2652.

6. Bolink, H. J.; Coronado, E.; Costa, R. D.; Lardies, N.; Orti, E., Near-Quantitative Internal Quantum Efficiency in a Light-Emitting Electrochemical Cell. *Inorg Chem* **2008,** 47, (20), 9149-51.

7. Chung, C. Y.-S.; Li, S. P.-Y.; Louie, M.-W.; Lo, K. K.-W.; Yam, V. W.-W., Induced Self-Assembly and Disassembly of Water-Soluble Alkynylplatinum(Ii) Terpyridyl Complexes with "Switchable" near-Infrared (Nir) Emission Modulated by Metal–Metal Interactions over Physiological Ph: Demonstration of Ph-Responsive Nir Luminescent Probes in Cell-Imaging Studies. *Chemical Science* **2013,** 4, (6), 2453-2462.

8. Baschieri, A.; Muzzioli, S.; Fiorini, V.; Matteucci, E.; Massi, M.; Sambri, L.; Stagni, S., Introducing a New Family of Biotinylated Ir(III)-Pyridyltriazole Lumophores: Synthesis, Photophysics, and Preliminary Study of Avidin-Binding Properties. *Organometallics* **2014,** 33, (21), 6154-6164.

9. Lo, K. K.-W.; Li, S. P.-Y., Utilization of the Photophysical and Photochemical Properties of Phosphorescent Transition Metal Complexes in the Development of Photofunctional Cellular Sensors, Imaging Reagents, and Cytotoxic Agents. *RSC Advances* **2014,** 4, (21).

10. Naddaka, M.; Locatelli, E.; Colecchia, D.; Sambri, L.; Monaco, I.; Baschieri, A.; Sasdelli, F.; Chiariello, M.; Matteucci, E.; Zani, P.; Franchini, M. C., Hybrid Cholesterol-Based Nanocarriers Containing Phosphorescent Ir Complexes: In Vitro Imaging on Glioblastoma Cell Line. *RSC Advances* **2015,** 5, (2), 1091-1096.

11. Nicewicz, D. A.; MacMillan, D. W., Merging Photoredox Catalysis with Organocatalysis: The Direct Asymmetric Alkylation of Aldehydes. *Science* **2008,** 322, (5898), 77-80.

12. Jin, J.; MacMillan, D. W., Alcohols as Alkylating Agents in Heteroarene C-H Functionalization. *Nature* **2015,** 525, (7567), 87-90.

13. Jeffrey, J. L.; Petronijevic, F. R.; MacMillan, D. W., Selective Radical-Radical Cross-Couplings: Design of a Formal Beta-Mannich Reaction. *J Am Chem Soc* **2015,** 137, (26), 8404-7.

14. Meyer, T. J., Optical and Thermal Electron Transfer in Metal Complexes. *Accounts Chem Res* **2002,** 11, (3), 94-100.

15. Zysman-Colman, E., *Iridium(III) in Optoelectronic and Photonics Applications*. John Wiley & Sons Ltd.: 2017.

16. Costa, R. D.; Orti, E.; Bolink, H. J.; Monti, F.; Accorsi, G.; Armaroli, N., Luminescent Ionic Transition-Metal Complexes for Light-Emitting Electrochemical Cells. *Angew Chem Int Edit* **2012,** 51, (33), 8178-8211.

17. Matteucci, E.; Baschieri, A.; Mazzanti, A.; Sambri, L.; Avila, J.; Pertegas, A.; Bolink, H. J.; Monti, F.; Leoni, E.; Armaroli, N., Anionic Cyclometalated Iridium(III) Complexes with a Bis-Tetrazolate Ancillary Ligand for Light-Emitting Electrochemical Cells. *Inorg Chem* **2017,** 56, (17), 10584-10595.

18. Hu, T.; He, L.; Duan, L.; Qiu, Y., Solid-State Light-Emitting Electrochemical Cells Based on Ionic Iridium(III) Complexes. *J Mater Chem* **2012,** 22, (10), 4206-4215.

19. Baranoff, E.; Bolink, H. J.; Constable, E. C.; Delgado, M.; Haussinger, D.; Housecroft, C. E.; Nazeeruddin, M. K.; Neuburger, M.; Orti, E.; Schneider, G. E.; Tordera, D.; Walliser, R. M.; Zampese, J. A., Tuning the Photophysical Properties of Cationic Iridium(III) Complexes Containing Cyclometallated 1-(2,4-Difluorophenyl)-1h-Pyrazole through Functionalized 2,2'-Bipyridine Ligands: Blue but Not Blue Enough. *Dalton Trans* **2013,** 42, (4), 1073-87.

20. Pal, A. K.; Krotkus, S.; Fontani, M.; Mackenzie, C. F. R.; Cordes, D. B.; Slawin, A. M. Z.; Samuel, I. D. W.; Zysman-Colman, E., High-Efficiency Deep-Blue-Emitting Organic Light-Emitting Diodes Based on Iridium(III) Carbene Complexes. *Adv Mater* **2018,** 30, (50), e1804231.

21. Grushin, V. V.; Herron, N.; LeCloux, D. D.; Marshall, W. J.; Petrov, V. A.; Wang, Y., New, Efficient Electroluminescent Materials Based on Organometallic Ir Complexes. *Chemical Communications* **2001,** (16), 1494-1495.

22. Pla, P.; Junquera-Hernandez, J. M.; Bolink, H. J.; Orti, E., Emission Energy of Azole-Based Ionic Iridium(III) Complexes: A Theoretical Study. *Dalton Trans* **2015,** 44, (18), 8497-505.

23. Giussani, A.; Pla, P.; Junquera-Hernandez, J. M.; Orti, E., Azole-Containing Cationic Bis-Cyclometallated Iridium(Iii) Isocyanide Complexes: A Theoretical Insight into the Emission Energy and Emission Efficiency. *Dalton Trans* **2019,** 48, (26), 9725-9733.

24. Tamayo, A. B.; Garon, S.; Sajoto, T.; Djurovich, P. I.; Tsyba, I. M.; Bau, R.; Thompson, M. E., Cationic Bis-Cyclometalated Iridium(III) Diimine Complexes and Their Use in Efficient Blue, Green, and Red Electroluminescent Devices. *Inorg Chem* **2005,** 44, (24), 8723-32.

25. Baranoff, E.; Fantacci, S.; De Angelis, F.; Zhang, X.; Scopelliti, R.; Gratzel, M.; Nazeeruddin, M. K., Cyclometalated Iridium(III) Complexes Based on Phenyl-Imidazole Ligand. *Inorg Chem* **2011,** 50, (2), 451-62.

26. Lai, W.-Y.; Levell, J. W.; Jackson, A. C.; Lo, S.-C.; Bernhardt, P. V.; Samuel, I. D. W.; Burn, P. L., A Phosphorescent Poly(Dendrimer) Containing Iridium(III) Complexes: Synthesis and Light-Emitting Properties. *Macromolecules* **2010,** 43, (17), 6986-6994.

27. Beyer, B.; Ulbricht, C.; Escudero, D.; Friebe, C.; Winter, A.; González, L.; Schubert, U. S., Phenyl-1h-[1,2,3]Triazoles as New Cyclometalating Ligands for Iridium(III) Complexes. *Organometallics* **2009,** 28, (18), 5478-5488.

28. Monti, F.; Baschieri, A.; Gualandi, I.; Serrano-Perez, J. J.; Junquera-Hernandez, J. M.; Tonelli, D.; Mazzanti, A.; Muzzioli, S.; Stagni, S.; Roldan-Carmona, C.; Pertegas, A.; Bolink, H. J.; Orti, E.; Sambri, L.; Armaroli, N., Iridium(III) Complexes with Phenyl-Tetrazoles as Cyclometalating Ligands. *Inorg Chem* **2014,** 53, (14), 7709-7721.

29. Kozhevnikov, V. N.; Dahms, K.; Bryce, M. R., Nucleophilic Substitution of Fluorine Atoms in 2,6-Difluoro-3-(Pyridin-2-Yl)Benzonitrile Leading to Soluble Blue-Emitting Cyclometalated Ir(III) Complexes. *J Org Chem* **2011,** 76, (12), 5143-8.

30. Kiplinger, J. L.; Richmond, T. G.; Osterberg, C. E., Activation of Carbon-Fluorine Bonds by Metal Complexes. *Chem Rev* **1994,** 94, (2), 373-431.

31. Sivasubramaniam, V.; Brodkorb, F.; Hanning, S.; Loebl, H. P.; van Elsbergen, V.; Boerner, H.; Scherf, U.; Kreyenschmidt, M., Fluorine Cleavage of the Light Blue Heteroleptic Triplet Emitter Firpic. *Journal of Fluorine Chemistry* **2009,** 130, (7), 640-649.

32. Gualandi, A.; Matteucci, E.; Monti, F.; Baschieri, A.; Armaroli, N.; Sambri, L.; Cozzi, P. G., Photoredox Radical Conjugate Addition of Dithiane-2-Carboxylate Promoted by an Iridium(Ii) Phenyl-Tetrazole Complex: A Formal Radical Methylation of Michael Acceptors. *Chem Sci* **2017,** 8, (2), 1613-1620.

33. Shavaleev, N. M.; Monti, F.; Scopelliti, R.; Armaroli, N.; Grätzel, M.; Nazeeruddin, M. K., Blue Phosphorescence of Trifluoromethyl- and Trifluoromethoxy-Substituted Cationic Iridium(III) Isocyanide Complexes. *Organometallics* **2012,** 31, (17), 6288-6296.

34. Shavaleev, N. M.; Monti, F.; Costa, R. D.; Scopelliti, R.; Bolink, H. J.; Orti, E.; Accorsi, G.; Armaroli, N.; Baranoff, E.; Gratzel, M.; Nazeeruddin, M. K., Bright Blue Phosphorescence from Cationic Bis-Cyclometalated Iridium(III) Isocyanide Complexes. *Inorg Chem* **2012,** 51, (4), 2263-71.

35. Shavaleev, N. M.; Monti, F.; Scopelliti, R.; Baschieri, A.; Sambri, L.; Armaroli, N.; Grätzel, M.; Nazeeruddin, M. K., Extreme Tuning of Redox and Optical Properties of Cationic Cyclometalated Iridium(III) Isocyanide Complexes. *Organometallics* **2013,** 32, (2), 460-467.

36. Ladouceur, S.; Fortin, D.; Zysman-Colman, E., Enhanced Luminescent Iridium(III) Complexes Bearing Aryltriazole Cyclometallated Ligands. *Inorg Chem* **2011,** 50, (22), 11514-26.

37. Donato, L.; Abel, P.; Zysman-Colman, E., Cationic Iridium(III) Complexes Bearing a Bis(Triazole) Ancillary Ligand. *Dalton T* **2013,** 42, (23), 8402-8412.

38. Ladouceur, S.; Fortin, D.; Zysman-Colman, E., Role of Substitution on the Photophysical Properties of 5,5'-Diaryl-2,2'-Bipyridine (Bpy*) in [Ir(Ppy)2(Bpy*)]Pf6 Complexes: A Combined Experimental and Theoretical Study. *Inorg Chem* **2010,** 49, (12), 5625-41.

39. Zhao, Y.; Truhlar, D. G., The M06 Suite of Density Functionals for Main Group Thermochemistry, Thermochemical Kinetics, Noncovalent Interactions, Excited States, and Transition Elements: Two New Functionals and Systematic Testing of Four M06-Class Functionals and 12 Other Functionals. *Theor Chem Acc* **2008,** 120, (1-3), 215-241.

40. Zhao, Y.; Truhlar, D. G., Density Functionals with Broad Applicability in Chemistry. *Accounts Chem Res* **2008,** 41, (2), 157-167.

41. Francl, M. M.; Pietro, W. J.; Hehre, W. J.; Binkley, J. S.; Gordon, M. S.; Defrees, D. J.; Pople, J. A., Self-Consistent Molecular-Orbital Methods .23. A Polarization-Type Basis Set for 2nd-Row Elements. *J Chem Phys* **1982,** 77, (7), 3654-3665.

42. Figgen, D.; Peterson, K. A.; Dolg, M.; Stoll, H., Energy-Consistent Pseudopotentials and Correlation Consistent Basis Sets for the 5d Elements Hf-Pt. *J Chem Phys* **2009,** 130, (16), 164108.

43. Tomasi, J.; Persico, M., Molecular-Interactions in Solution - an Overview of Methods Based on Continuous Distributions of the Solvent. *Chem Rev* **1994,** 94, (7), 2027-2094.

44. Tomasi, J.; Mennucci, B.; Cammi, R., Quantum Mechanical Continuum Solvation Models. *Chem Rev* **2005,** 105, (8), 2999-3093.

45. Cramer, C. J.; Truhlar, D. G., Continuum Solvation Models. In *Solvent Effects and Chemical Reactivity*, Tapia, O.; Bertrán, J., Eds. Springer Netherlands: 2002; Vol. 17, pp 1-80.

46. De Angelis, F.; Fantacci, S.; Evans, N.; Klein, C.; Zakeeruddin, S. M.; Moser, J. E.; Kalyanasundaram, K.; Bolink, H. J.; Gratzel, M.; Nazeeruddin, M. K., Controlling Phosphorescence Color and Quantum Yields in Cationic Iridium Complexes: A Combined Experimental and Theoretical Study. *Inorg Chem* **2007,** 46, (15), 5989-6001.

47. Monti, F.; Baschieri, A.; Matteucci, E.; Mazzanti, A.; Sambri, L.; Barbieri, A.; Armaroli, N., A Chelating Diisocyanide Ligand for Cyclometalated Ir(III) Complexes with Strong and Tunable Luminescence. *Faraday Discuss* **2015,** 185, 233-48.

48. Constable, E. C.; Neuburger, M.; Rosel, P.; Schneider, G. E.; Zampese, J. A.; Housecroft, C. E.; Monti, F.; Armaroli, N.; Costa, R. D.; Orti, E., Ligand-Based Charge-Transfer Luminescence in Ionic Cyclometalated Iridium(III) Complexes Bearing a Pyrene-Functionalized Bipyridine Ligand: A Joint Theoretical and Experimental Study. *Inorg Chem* **2013,** 52, (2), 885-97.

49. Martin, R. L., Natural Transition Orbitals. *J Chem Phys* **2003,** 118, (11), 4775-4777.

50. Ladouceur, S.; Swanick, K. N.; Gallagher-Duval, S.; Ding, Z.; Zysman-Colman, E., Strongly Blue Luminescent Cationic Iridium(III) Complexes with an Electron-Rich Ancillary Ligand: Evaluation of Their Optoelectronic and Electrochemiluminescence Properties. *Eur J Inorg Chem* **2013,** 2013, (30), 5329-5343.

51. Crosby, G. A.; Demas, J. N., Measurement of Photoluminescence Quantum Yields. Review. *The Journal of Physical Chemistry* **1971,** 75, (8), 991-1024.

52. Meech, S. R.; Phillips, D., Photophysics of Some Common Fluorescence Standards. *Journal of Photochemistry* **1983,** 23, (2), 193-217.

53. Wurth, C.; Grabolle, M.; Pauli, J.; Spieles, M.; Resch-Genger, U., Relative and Absolute Determination of Fluorescence Quantum Yields of Transparent Samples. *Nat Protoc* **2013,** 8, (8), 1535-1550.

54. Frisch, M. J.; Trucks, G. W.; Schlegel, H. B.; Scuseria, G. E.; Robb, M. A.; Cheeseman, J. R.; Scalmani, G.; Barone, V.; Petersson, G. A.; Nakatsuji, H.; Li, X.; Caricato, M.; Marenich, A. V.; Bloino, J.; Janesko, B. G.; Gomperts, R.; Mennucci, B.; Hratchian, H. P.; Ortiz, J. V.; Izmaylov, A. F.; Sonnenberg, J. L.; Williams; Ding, F.; Lipparini, F.; Egidi, F.; Goings, J.; Peng, B.; Petrone, A.; Henderson, T.; Ranasinghe, D.; Zakrzewski, V. G.; Gao, J.; Rega, N.; Zheng, G.; Liang, W.; Hada, M.; Ehara, M.; Toyota, K.; Fukuda, R.; Hasegawa, J.; Ishida, M.; Nakajima, T.; Honda, Y.; Kitao, O.; Nakai, H.; Vreven, T.; Throssell, K.; Montgomery Jr., J. A.; Peralta, J. E.; Ogliaro, F.; Bearpark, M. J.; Heyd, J. J.; Brothers, E. N.; Kudin, K. N.; Staroverov, V. N.; Keith, T. A.; Kobayashi, R.; Normand, J.; Raghavachari, K.; Rendell, A. P.; Burant, J. C.; Iyengar, S. S.; Tomasi, J.; Cossi, M.; Millam, J. M.; Klene, M.; Adamo, C.; Cammi, R.; Ochterski, J. W.; Martin, R. L.; Morokuma, K.; Farkas, O.; Foresman, J. B.; Fox, D. J. *Gaussian 16, Rev. B.01*, Gaussian Inc.: Wallingford, CT, USA, 2016.

55. Stratmann, R. E.; Scuseria, G. E.; Frisch, M. J., An Efficient Implementation of Time-Dependent Density-Functional Theory for the Calculation of Excitation Energies of Large Molecules. *J Chem Phys* **1998,** 109, (19), 8218-8224.

56. Casida, M. E.; Jamorski, C.; Casida, K. C.; Salahub, D. R., Molecular Excitation Energies to High-Lying Bound States from Time-Dependent Density-Functional Response Theory: Characterization and Correction of the Time-Dependent Local Density Approximation Ionization Threshold. *J Chem Phys* **1998,** 108, (11), 4439-4449.

57. Bauernschmitt, R.; Ahlrichs, R., Treatment of Electronic Excitations within the Adiabatic Approximation of Time Dependent Density Functional Theory. *Chem Phys Lett* **1996,** 256, (4-5), 454-464.

58. Dennington, R.; Keith, T. A.; Millam, J. M. *Gaussview, Version 6*, Semichem Inc.: Shawnee Mission, KS, USA, 2016.

59. Humphrey, W.; Dalke, A.; Schulten, K., Vmd: Visual Molecular Dynamics. *J Mol Graph Model* **1996,** 14, (1), 33-38.

Highly-energetic iridium(III) complexes with fluorinated tetrazole ligands
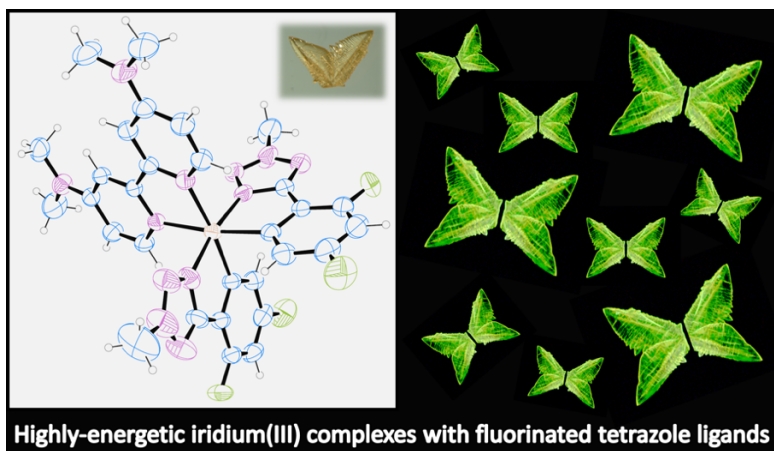
A series of cationic iridium(III) complexes equipped with fluorinated phenyl-tetrazole cyclometalating ligands is reported. These molecules display blue emission from ligand-centered excited states, displaying long lifetimes (up to 43 μs in oxygen-free acetonitrile solution at 298 K). Such photophysical behavior is radically different from that of their non-fluorinated analogues previously reported, making this novel class of complexes very promising as photoredox catalysts.